Supplementary Information

SERS sensing chip based on Ti_3C_2/nano-Au@MA for ultrasensitive amine gas detection

Liwei Hou[a,c], Xinyue Xu[a, b], Xiaoli Wang[a,b], Li Wang[a,b], Fengchun Tian[**d], Yi Xu*[a,b]

[a] Key Laboratory of Optoelectronic Technology & System, Ministry of Education, Chongqing University, Chongqing 400044, China;

[b] College of Optoelectronic Engineering, Chongqing University, Chongqing 400044, China;

[c] College of Chemistry and Chemical Engineering, Chongqing University, Chongqing 400044, China;

[d] College of Microelectronic and Communication Engineering, Chongqing University, Chongqing 400044, China;

* Corresponding author at: Key Disciplines Lab of Novel Micro-Nano Devices and System Technology, Chongqing University, No. 174, St. Shazhengjie, Shapingba District, Chongqing, 400044, China; E-mail address: xuyibbd@cqu.edu.cn (Y. Xu)

** Corresponding author at: College of Microelectronic and Communication Engineering, Chongqing University, Chongqing 400044, China; E-mail： fengchuntian@cqu.edu.cn

1. Schematic diagram of amine gas sensing test flow by the QCM sensor and Ti_3C_2/nano-Au@MA SERS chip

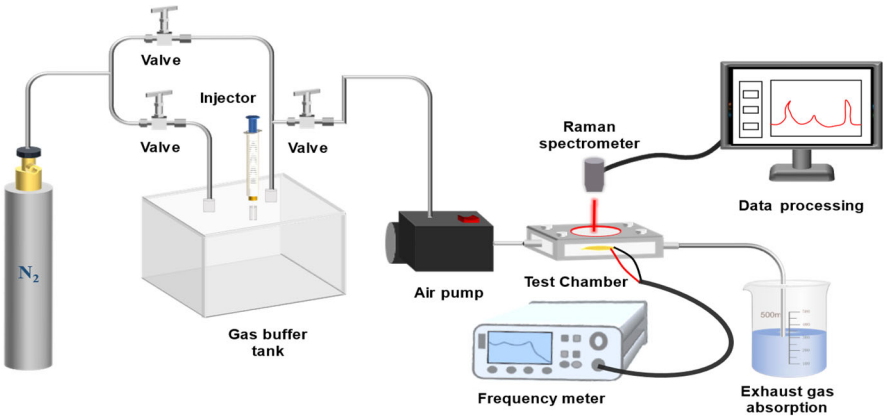

Figure S1. Schematic diagram of amine gas sensing test flow.

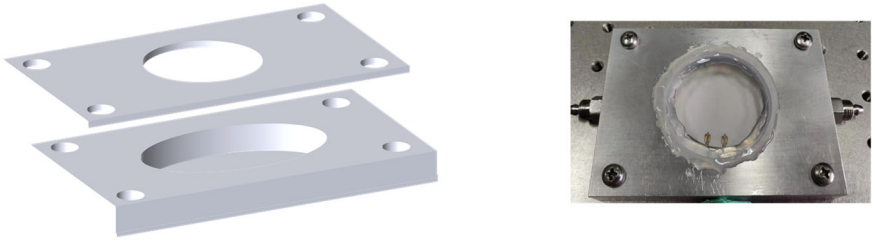

Figure S2. Detection chamber for gas SERS spectroscopy

2. Electromagnetic field simulation of Au nanoparticles with different shapes

According to the theory of surface-enhanced Raman spectroscopy, the enhancement factor is closely related to the structural morphology and incident wavelength of nanomaterials. In this work, COMSOL was adopted to simulate the electromagnetic field of gold nanoparticles with different shapes. The different morphologies of particles prepared in the experiments were simplified and modeled in four shapes: spherical, ellipsoidal, cubic, and rhombic conical, with a diameter size of 100 nm and an incident wavelength of 785 nm. All the simulations were performed with a normal-size mesh and 1 V/m incident electric field.

It was shown that the enhancement factor was closely related to the structural shape of the nanoparticles and the incident wavelength of 785 nm in the simulations of single nanoparticles. It was also illustrated that the spherical nanoparticles had the largest enhancement effect at an incident wavelength of 785 nm compared to other geometries. When the particle size and incident wavelength were at resonance and Mie scattering was considered, spherical nanoparticle monoliths were of the maximum LSPR. Spherical nanoparticles were most commonly used for the preparation of SERS substrates as it resonated easily in the incident wavelength range. It was also found that nano-Au with a spherical shape had the best detection from further SERS testing experiments.

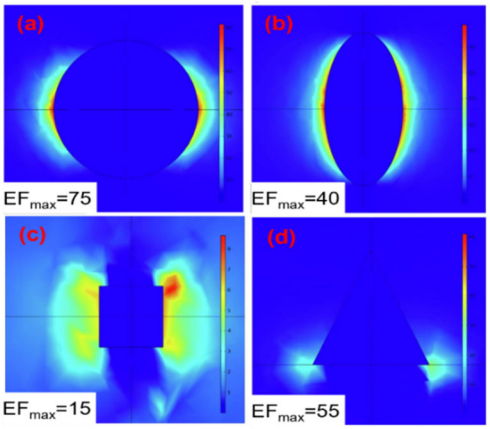

Figure S3. Electromagnetic field enhancement maps for different shapes of single Au nanoparticles at 785 nm incident wavelength: (a) Spherical, (b) Spheroid, (c) Cubical, (d) Rhombic cone shapes, respectively.

3. Calculation of the enhancement factor

Enhancement factor calculated: By the following equation[1]:

$$AEF = (I_{sers}/N_{ads})/(I_{bulk}/N_{bulk}) \quad (1)$$

In equation (1), N_{ads} and N_{bulk} represent the number of R6G molecules in the SERS sample and the normal Raman sample, respectively. Similarly, I_{SERS} and I_{bulk} are the same vibration peak of R6G molecule on a single Ti_3C_2/Au particle and the normal Raman spectrum from a solid sample, respectively. The laser spot size is about 0.91 μm^2, and the depth of laser penetration is about 22 μm. The density of R6G solid is about 1.15 g cm^{-3}, and N_{bulk} was estimated to be around 5×10^{10}. N_{ads} is determined by illuminating the laser spot on the sample and calculating the density of the R6G molecule adsorbed on the single Ti_3C_2/Au surface, which is approximately 0.5 nM cm^{-2}. I_{SERS} and I_{bulk} are based on the R6G molecule vibration peak at 1356 cm^{-1} in the SERS spectrum and the normal Raman spectrum shown in **Figure S5**. The intensity was obtained by averaging 20 laser spot measurements, where I_{SERS} = 20200 and I_{bulk} = 875, while also considering the laser power for SERS and normal Raman.

Table S4. Comparison of the calculated enhancement factors (EF) of R6G between different SERS substrates.

Substrate	Sensitivity	EF
nano-Au	10^{-5} M	2.4×10^{6}
Ti_3C_2	10^{-2} M	1.2×10^{3}
Ti_3C_2/nano-Au	10^{-7} M	1.7×10^{10}

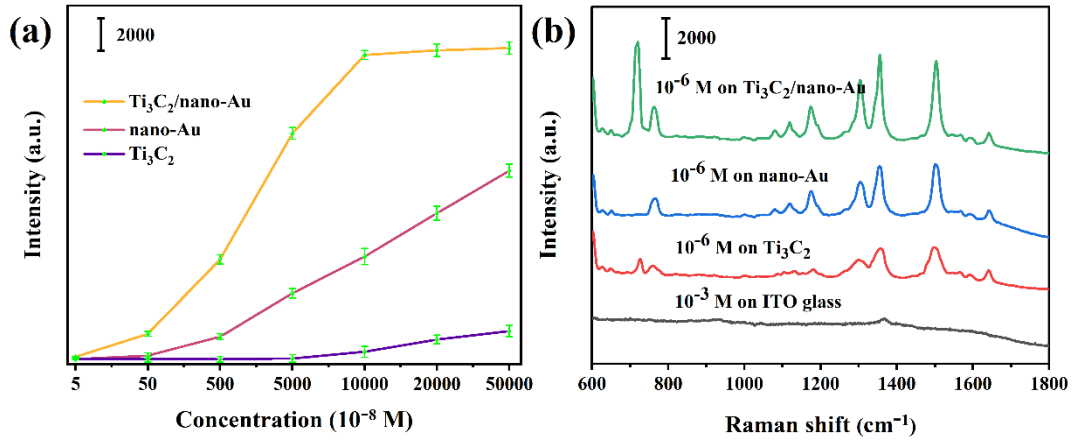

Figure S5. (a) The relationship of peak intensities at 1356 cm^{-1} and concentrations of R6G adsorbed on different SERS substrates. (b) Raman spectra of 1 mM R6G on glass and 1 μM R6G on the different SERS substrates; Power: 0.8 mW for SERS, Lens: 100 × objective.

4. Ti_3C_2 adsorption performance test on amine gas by the QCM sensor

A frequency meter was used to monitor the frequency shift of the QCM during the process of adsorbing ammonia, and then the adsorption capacity of the Ti_3C_2 for amine gas could be obtained quantitatively. The relationship between the adsorption amount (m) and the frequency shift (ΔF) was expressed using the Sauerbrey equation[2]:

$$\Delta m = -\frac{A\sqrt{\mu_q \mu \rho_q}}{2f_0^2} \cdot \Delta f = -c \cdot \Delta f \quad (2)$$

where μ_q is the shear modulus of quartz (μ_q = 2.947 × 1011 dyn/cm^2), ρ_q is the density of quartz (ρ_q= 2.648 g/cm^3), A is the effective sensitive area of QCM (A = 1.1304 cm^2), and f_0 is the base frequency of QCM (9 MHz).

The base frequency of QCM stabilized at a constant value under the nitrogen atmosphere; however, it decreased to a constant value after the introduction of amine gas and gradually returned to its base value after the reintroduction of high-purity nitrogen. The frequency shifts that occurred between the introduction and removal of amine gas were used as the detection signals.

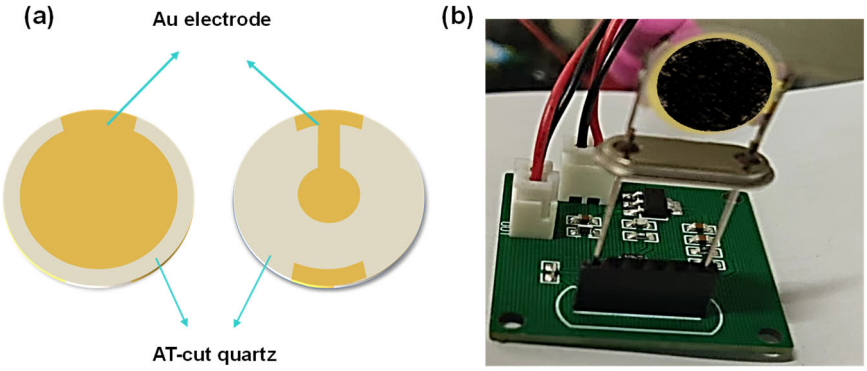

Figure S6. Amine gas detection method based on QCM. (a) Schematic diagram of the front and back of QCM quartz chip. (b) Ti_3C_2@QCM physical drawing of the sensor chip.

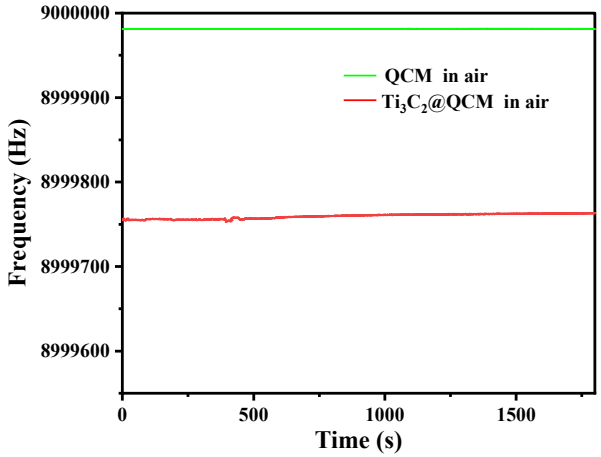

Figure S7. Change of baseline frequency in air before and after Ti_3C_2 loading.

5. SEM image of nano-Au@ITO with different morphology

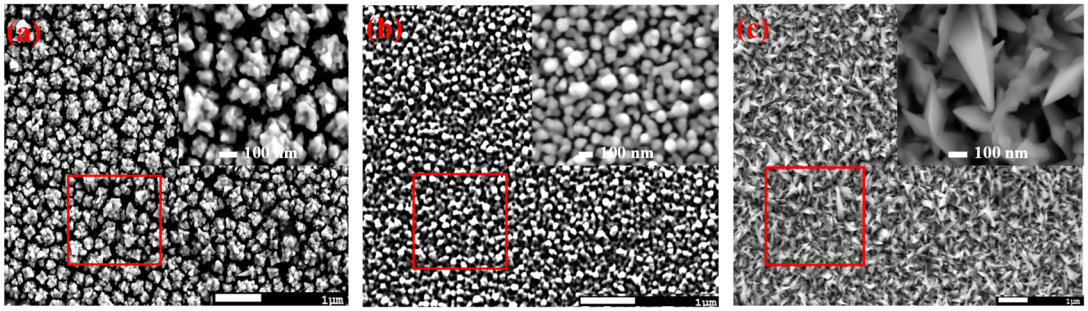

Figure S8. (a) SEM image of nano-Au@ITO with rhombic cone-shape, (b) SEM image of nano-Au@ITO with spherical shape, (c) SEM image of nano-Au@ITO with coral-like shape.

6. TEM image of Ti_3C_2/nano-Au

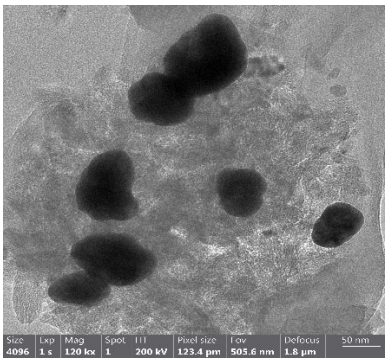

Figure S9. TEM image of Ti_3C_2/nano-Au

7. Raman spectrum of Ti_3C_2

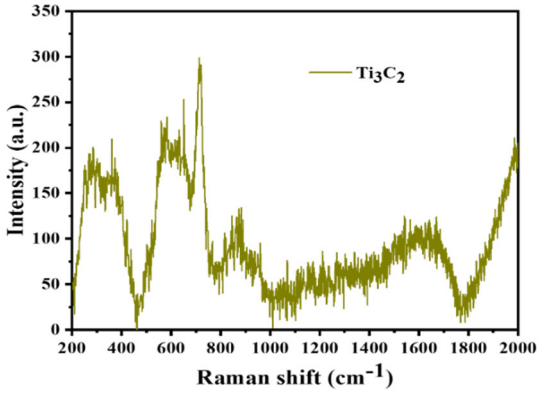

Figure S10. Raman spectrum of Ti_3C_2, Power: 10 mW for SERS, Lens: 100 × objective.

8. Detection of 13.8 ppm of aniline on Ti_3C_2/nano-Au@MA SERS substrates fabricated using nanometer-sized gold with various morphologies.

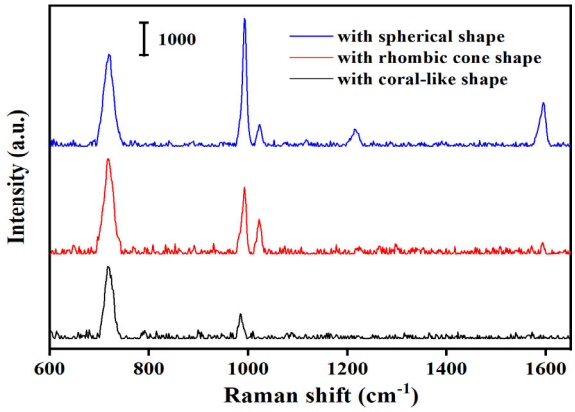

Figure S11. Detection of 13.8 ppm aniline gas by Ti_3C_2/nano-Au@MA enhanced SERS substrate.

9. Raman spectra of aniline, p-phenylenediamine and diethylamine

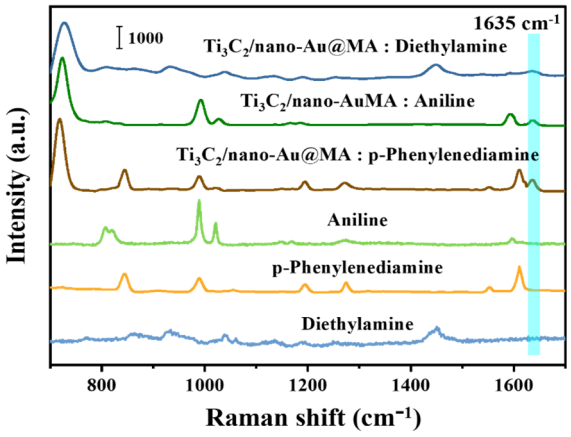

Figure S12. Raman spectra of aniline, p-phenylenediamine, and diethylamine and SERS spectra of Ti_3C_2/nano-Au@MA SERS in the presence of three gases (1 ppm)

10. Detection of different concentrations of p-phenylenediamine and diethylamine by Ti_3C_2/nano-Au@MA SERS chip

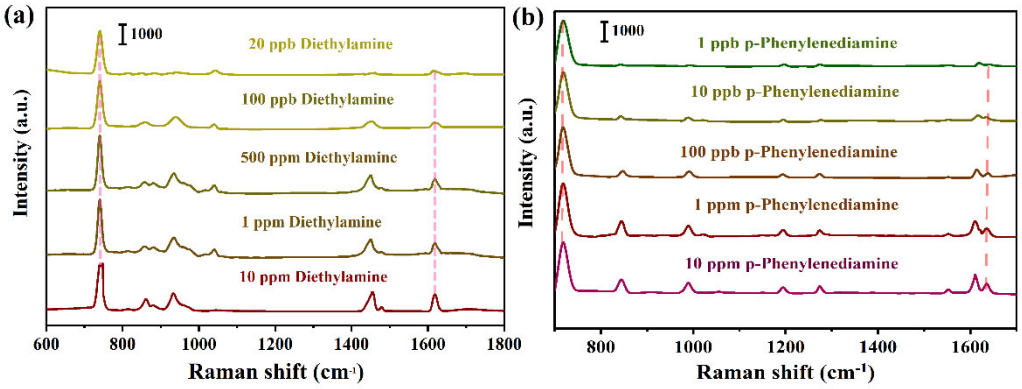

Figure S13. SERS spectra measured from Ti_3C_2/nano-Au@MA SERS chip for diethylamine and p-phenylenediamine gaseous molecules.

11. Repeatability testing of Ti_3C_2/nano-Au@MA SERS chip for aniline

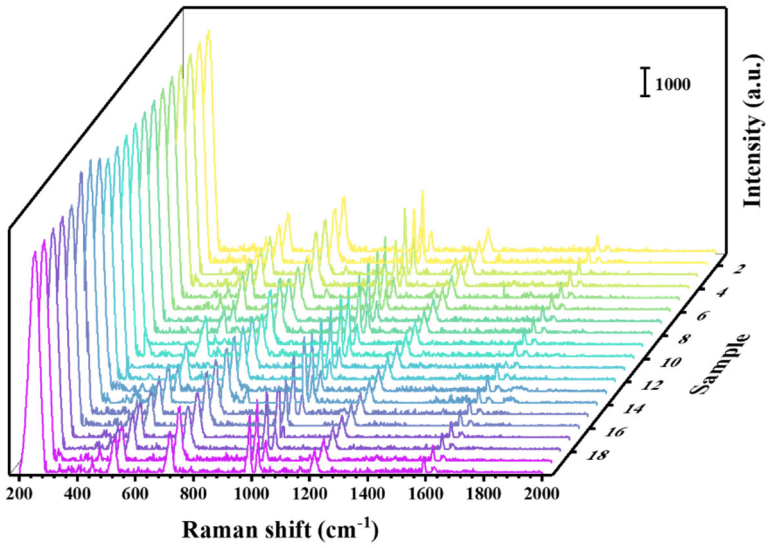

Figure S14. SERS spectra of 20 tests for 1 ppm aniline using Ti_3C_2/nano-Au@MA SERS chip.

12. Calculation of gas mixture composition ratio

To determine the composition ratio of gases experimentally, we utilized the SERS signals acquired with Ti_3C_2/nano-Au@MA as a Raman signal amplifier. As mentioned in earlier papers[3-5], the correlation between SERS intensity and concentration can be represented by the following equation.

$$I \propto logC \qquad (3)$$

Where I is the intensity of SERS and C is the concentration of gas molecules. As previously reported[6], the intensity varies depending on the target and is not affected by other factors. Thus, when two target gas molecules 1 and 2 are placed on the surface, the intensity of each gas molecule can be expressed as

$$I_{1,\,mix} = a_1 \bullet logC_1 + Y_1 \qquad (4)$$

$$I_{2,\,mix} = a_2 \bullet logC_2 + Y_2 \qquad (5)$$

where a is the coefficient of proportionality between intensity and the logarithm of concentration and Y_1 and Y_2 are y-intercepts. To compare the concentration of each gas, intensity (N) can be divided by each coefficient (slope, k). For instance, for the target molecule 1, the equation can be rearranged as

$$N_1 = I_1 / a_1 = logC_1 + Y_1 / a_1 \qquad (6)$$

and that for molecule 2 can be expressed as

$$N_2 = I_2 / a_2 = logC_2 + Y_2 / a_2 \qquad (7)$$

Confirmation of the linear relationship between the difference in normalized intensity and the log of concentration ratio is possible through these relationships, as expressed by

$$\Delta I_R = N_1 - N_2 = \log(C_1/C_2) + Y_1/a_1 - Y_2/a_2 \qquad (8)$$

As a result, the ratio in the mixed gas can be calculated by each gas SERS intensity.

13. Stability testing of Ti_3C_2/nano-Au@MA SERS sensing chip

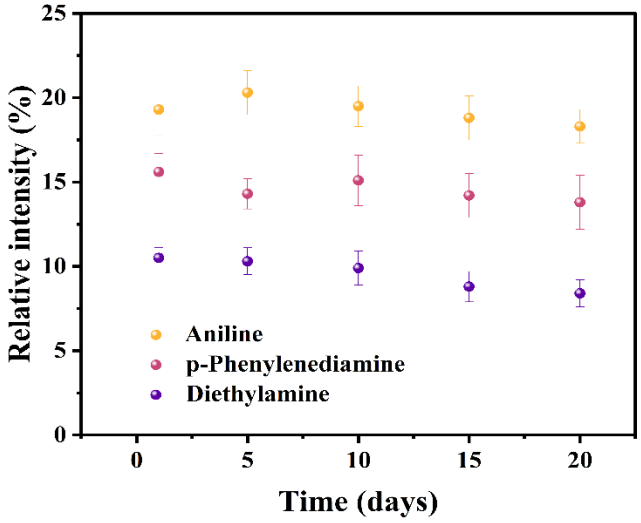

Figure S15. Stability test over 20 days

14. Reliability testing

Table S16. The recoveries for amine in the air sample by determination using Ti_3C_2/nano-Au@MA SERS sensor

Sample	Amine content in sample (mg m^{-3})	Spiked level (mg m^{-3})	Found level (mg m^{-3})	Recovery (±RSD), n=3
Air/aniline	0.42	0.30	0.68	88.88% ± 1.88%
		1.50	1.90	99.20% ± 1.33%
		3.00	3.67	109.18% ± 1.91%
Air/ p-phenylenediamine	0.51	0.30	6.65	89.75% ± 2.58%
		1.50	2.15	107.11% ± 1.28%
		3.00	3.66	106.15% ± 1.62%
Air/diethylamine	0.35	0.30	0.56	92.90% ± 1.98%
		1.50	1.89	98.01% ± 2.99%
		3.00	3.62	108.18% ± 2.71%

15. Actual polluted air sample testing

On-site sampling was carried out in the aerobic tank of a pharmaceutical company's wastewater treatment station, and two samples were taken at the upwind and downwind outlets named Sample 1 and Sample 2 respectively and then brought back to the laboratory for testing and comparison with unpolluted air. Each of the three gases was passed into the detection chamber with Ti_3C_2/nano-Au@MA for 10 min, and SERS spectroscopy was performed after sufficient adsorption.

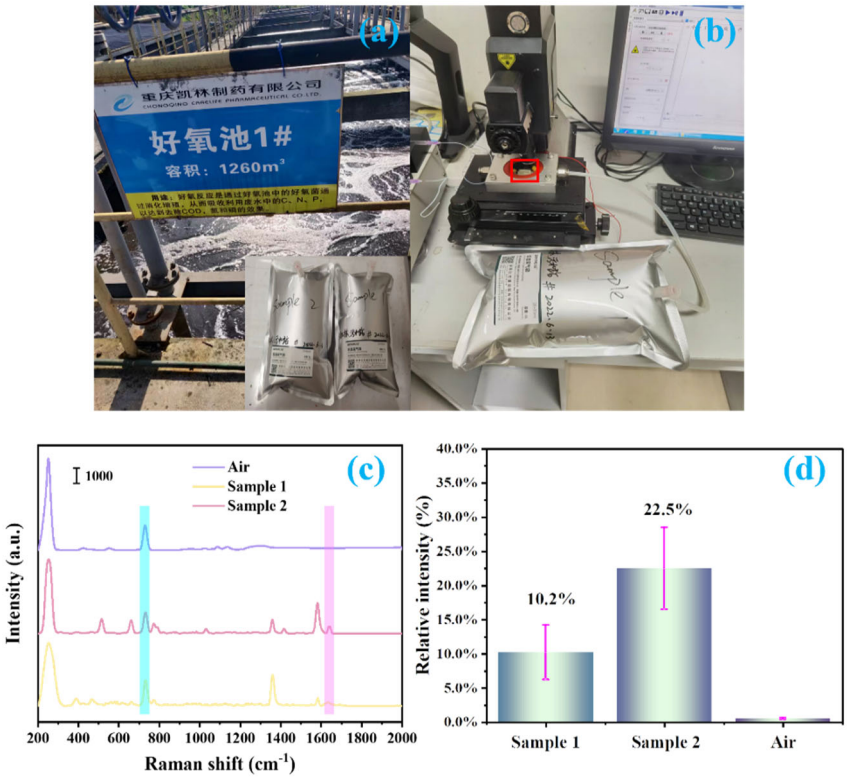

Figure S17. (a) gas sample collection site, (b) test charts on gas samples, (c) SERS spectra of the three collected gases, and (d) I_{1635}/I_{724} intensity comparison of the SERS spectra of the three gas samples.

Table S18. Comparison of GC-MS and SERS sensor methods for detecting the amine in different samples.

Samples	**Found level for GC-MS (mg m^{-3})**	**Found level for SERS sensor (mg m^{-3}), n=3**
Samlpe 1	0.19 ± 0.05	0.17 ± 0.11
Sample 2	1.95 ± 0.12	1.87 ± 0.22
Air	0.01 ± 0.01	0.01 ± 0.01

References

1. J. Quan, J. Zhang, J. Li, X. Zhang, M. Wang, N. Wang and Y. Zhu, *Carbon*, 2019, **147**, 105-111.https://doi.org/10.1016/j.carbon.2019.02.077
2. Q. Zhou, L. Zhu, C. Zheng and J. Wang, *ACS Appl. Mater. Interfaces*, 2021, **13**, 41339-41350.https://doi.org/10.1021/acsami.1c12213
3. X. Qiao, B. Su, C. Liu, Q. Song, D. Luo, G. Mo and T. Wang, *Adv. Mater.*, 2018, **30,** 1702275.https://doi.org/10.1002/adma.201702275
4. K. M. Baek, J. Kim, S. Kim, S. H. Cho, M. S. Jang, J. Oh and Y. S. Jung, *Chem. Mater.*, 2018, **30**, 6183-6191.https://doi.org/10.1021/acs.chemmater.8b02995
5. L. Xu, W. Yan, W. Ma, H. Kuang, X. Wu, L. Liu, Y. Zhao, L. Wang and C. Xu, *Adv. Mater.*, 2015, **27**, 1706-+.https://doi.org/10.1002/adma.201402244
6. D. Zhang, L. Huang, B. Liu, H. Ni, L. Sun, E. Su, H. Chen, Z. Gu and X. Zhao, *Biosens. Bioelectron.*, 2018, **106**, 204-211.https://doi.org/10.1016/j.bios.2018.01.062